CONF-9106236--2

ANL/CP--73164

DE92 003402

MAR 1 0 1992

Atomic Structure of Heterophase Interfaces*

K.L. Merkle, M.I. Buckett, and Y. Gao
Materials Science Division
Argonne National Laboratory, Argonne, IL 60439 USA

The submitted manuscript has been authored by a contractor of the U.S. Government under contract No. W-31-109-ENG-38. Accordingly, the U.S. Government retains a nonexclusive, royalty-free license to publish or reproduce the published form of this contribution, or allow others to do so, for U.S. Government purposes.

MASTER

*Work supported by the U.S. Department of Energy, BES-Materials Sciences, under Contract No. W-31-109-Eng-38.

Manuscript submitted to the ***International Symposium on Metal/Ceramic Interfaces***, Irsee, Germany, June 30-July 5, 1991.

Atomic Structure of Heterophase Interfaces

K. L. Merkle, M. I. Buckett and Y. Gao

Materials Science Division

Argonne National Laboratory

Argonne, IL 60439 USA

Abstract ---High-resolution electron microscopy (HREM) has been used to study internal interfaces between dissimilar materials, notably ceramic/metal interfaces. Structures observed for systems with small and large misfits are compared in metal/metal, metal/ceramic, and ceramic/ceramic boundaries. The interfaces were prepared by a variety of techniques, including internal reduction, internal oxidation, and epitaxial growth by MOCVD and special thin-film techniques. While interfaces produced by internal oxidation and reduction in fcc systems typically form boundaries on (111) planes, non-equilibrium boundaries have also been generated using special thin film techniques. All boundaries can be characterized by their tendency to form coherent structures. While it appears that the amount of misfit and the bond strength primarily determine the degree of coherency, kinetic factors and substrate defects also seem to play an important role in determining the local defect structure at the boundary and the type of misfit localization.

1. Introduction

The unavoidable atomic disorder at a heterophase interface, which is due to different lattice parameters and/or structures on the opposing sides of the interface, necessarily gives rise to the formation of defect structures which seek to accommodate the mismatch at the interface. The mechanical strength and other properties of heterophase interfaces must ultimately be related to the atomic structure and the atomic interactions at the interface.

Obviously, observations which relate to the atomic structure of such interfaces are important for an understanding of the connection between properties and microstructure. Also, simple concepts about the formation and the atomic interactions at such interfaces may be elucidated by such studies. High-resolution electron microscopy (HREM) has been shown to be a valuable tool for atomic-level examination of metal/ceramic and other heterophase interfaces [1, 2].

The present paper is concerned with the HREM observation of a number of heterophase interfaces, which differ by their misfit, crystal structure, boundary type, and method of preparation. We report here on simple systems which do not form reaction layers at the interface. Most of this work is concerned with fcc metal/metal-oxide systems which have a range of misfits up to relatively large values. Observations on metal/metal and ceramic/ceramic systems are also included for comparison.

It is found that for practically all systems investigated a strong tendency exists to establish coherence of atomic planes across the interface. For interfaces produced under equilibrium conditions, the interface is typically formed by atomically dense-packed planes. The detailed structure of interfacial defects depends on the misfit and the degree of misfit localization.

2. Experimental

2.1. Specimen preparation

To produce interfaces that could be studied by HREM techniques, the specimens were prepared by a variety of techniques:

2.1.1. Metal/ceramic interfaces produced by precipitation:

Copper precipitates were prepared by internal reduction using the following procedure: The amorphous citrate process was used to prepare 10% Cu doped NiO powder. Polycrystalline boules were grown by the Verneuil process in an arc-image furnace. Thin slices cut from the (Ni,Cu)O boule were annealed at 1273 K for several days in a CO_2/CO atmosphere. A CO_2/CO ratio near 100 gave reducing conditions for Cu, but not for NiO and resulted in the precipitation of Cu.

Oxide precipitates in a metal matrix were prepared from Pd alloys by internal oxidation. Anneals of $PdNi_{0.03}$ in air in the range 973-1273 K and for periods between 3 and 17 hrs produced NiO precipitates. The precipitates were further annealed for several hours at 1173 K in a Ar, 0.2% O_2 atmosphere which resulted in well-developed planar interfaces suitable for HREM investigations.

2.1.2. Metal/ceramic and metal/metal interfaces produced by thin film techniques:

Special thin film techniques for the preparation of heterophase interfaces were developed and applied for investigations of the NiO/Ag, NiO/Au, MgO/Au, Ni/Au, and Ni/Ag systems. Briefly, for the Ni based interfaces composite epitaxial thin films, consisting of Ni particles embedded in the matrix of the other component, were used. The films were annealed after removal from the substrate and in this manner the interface was free to choose a low-energy equilibrium configuration [3, 4]. The metal/oxide interfaces were formed by external oxidation of the particle/matrix thin films. Interfaces whose orientation did typically not correspond to a low-energy configuration were produced for

the MgO/Au system. Here, small MgO smoke particles were collected (in more or less random orientations around their <001> axis) on (011) NaCl substrates that served as templates for (011) epitaxially grown Au films. The anneals at temperatures near 600 K were sufficient to form a bond between the MgO particles and the metal film, but did not affect the original orientation of the MgO, thus resulting in more or less random interfaces, subject to the above constraints.

2.1.3. Ceramic/Ceramic interfaces produced by MOCVD:

TiO_2 thin films were prepared in a cold-wall horizontal low-pressure metal-organic chemical vapor deposition (MOCVD) system. Titanium isopropoxide ($Ti(OC_3H_7)_4$) was used as metal-organic precursor. The precursor vapor was introduced into the reactor by high-purity nitrogen as carrier gas. The TiO_2 thin films were grown on $(11\bar{2}0)$ α-Al_2O_3 at 800 °C. Other growth parameters have been described in detail elsewhere [5].

2.2. TEM observations

Mechanical dimpling was used to pre-thin bulk specimen to a thickness of 15 to 30 μm. Both oxide and metal samples suitable for TEM observation were obtained by ion-milling on a liquid nitrogen cooled stage. HREM micrographs were taken under axial illumination near the optimum defocus $\Delta_F = (1.5C_s\lambda)^{1/2}$, where C_s is the spherical aberration constant of the objective lens and λ is the electron wavelength, using a H9000 high-resolution electron microscope operated at 300 kV.

3. HREM of Interface Structure

Interfaces ideally suited for atomic resolution microscopy must fulfill two basic geometric conditions. First, the two solids on opposite sides of the interfaces must have

low-index zone axes parallel to each other for a direct interpretation of HREM images in terms of the positions of atomic columns. Secondly, the atomic positions of the interfacial defects must be confined to displacements that largely preserve atomic columns which are parallel to the electron beam. Only if both conditions are fulfilled a simple interpretation of the observed structures as projections of atomic columns is possible. While the first condition is always ideally fulfilled in interfaces with suitable epitaxial or topotactical relationships, the second condition is not satisfied if, as is common for heterophase boundaries, a two-dimensional network of misfit dislocations exists at the interface. Particularly for dislocations inclined to the viewing direction the structure of the dislocation core is not directly accessible from HREM images, but comparisons can be made to theoretical models when available [3]. Fortunately, in cases where the displacements are weak or when the misfit is small, quite distinct and qualitatively interpretable atomic column contrasts can often be obtained. Nevertheless, even such qualitative interpretations must always be guided by results from image simulations.

3.1. Interface Geometry

The precipitate morphology in all fcc systems investigated here is largely determined by the formation of (111) interfaces, in agreement with previous TEM and HREM observations on fcc systems [6 - 10]. Figures 1 -3 show precipitates in the cube-on-cube orientation viewed along $\langle 0\bar{1}1 \rangle$. Octahedral shapes defined by the possible (111) boundaries in the cube-on-cube orientation are approximated by the precipitates with different degrees of perfection. While NiO precipitates have quite sharp corners where the (111) faces meet (see Fig. 3), others generally have rounded corners or are truncated at (100) planes. Macroscopically rounded corners typically are clearly microfaceted on an atomic scale, often displaying a step length that is commensurate to the quasiperiod of the interface [11]. In addition to the cube-on-cube oriented precipitates, twin-related precipitates are found in Pd/NiO. These precipitates are readily recognized by their

elongated shape along the (111) planes. Several low index symmetric and asymmetric interfaces such as (211)(211), (111)(511), and (100)(122) have been observed to form minor facets in these precipitates [11].

Interfaces formed by thin film techniques consist of islands of one phase embedded into the other phase. Since the geometry of the original islands (i.e. Ni in the Ni-based systems and MgO in the smoke-particle experiment) are not necessarily in an equilibrium configuration, the shapes observed after annealing may be indicative of low-energy boundaries, provided that the equilibrium can be approached. This is clearly not the case for the smoke-particle experiment, since the annealing temperature was too low to change the precipitate shape or orientation. However, in Ni/Ag, Ni/Au, NiO/Ag,and NiO/Au the (111) faces have been found to be clearly preferred. For Ni/Ag this is demonstrated in Fig. 4, which shows the reconstruction of a (110) boundary into (111) microfacets.

MOCVD grown rutile (R) films (TiO_2) on $(11\bar{2}0)$ sapphire (S) (α-Al_2O_3) have the epitaxial orientation relationship : $(101)\langle 010\rangle_R \| (11\bar{2}0)\langle 0001\rangle_S$. Growth twins are commonly observed in the films with (101) twin planes and <101> twinning directions [12, 13]. Note that also in this case of a heterostructural interface dense-packed atomic planes form at the interface.

3.2. Coherence and Boundary Geometry

The interfacial energy and the binding force between heterophase materials must depend on the interactions at the atomic level. Strong interatomic interactions favor the alignment of atoms across the interface. Thus the misfit owing to different lattice parameters and/or structures is not distributed uniformly, but is localized to regions of misfit, typically in the form of a two-dimensional network of misfit dislocations.

Table 1 summarizes the misfits associated with the systems that have been investigated here. A limited amount of information on the geometry of the misfit dislocation networks can be extracted from HREM observations. While the presence of a

quasiperiodic structural modulation along the interface and normal to the electron beam is quite obvious in all of the investigated interfaces (see Figs. 1 - 7), the period often shows slight variations (typically less than 10 %) from the ideal geometric repeat distance. This may indicate the presence of residual strains associated with the precipitates. It is important to note that all of the interfaces indicate the existence of misfit dislocations, however the degree of misfit localization varies, as discussed below.

Whenever there is only a small amount of misfit, such as for NiO/Ag, NiO/Au and for $<10\bar{1}>_R$ in the rutile/sapphire interface, the HREM observations clearly show the coherence between most of the lattice planes crossing the interface (see Figs. 4 and 8). At large misfits, the coherence which exists between some of the lattice planes is often not very obvious, particularly when the dislocation cores appear somewhat delocalized, such as in Figs. 1 and 5. A considerable tendency for maintaining coherence between lattice planes is also noticeable in the interfaces produced between MgO smoke particles and epitaxially grown Au films (see Fig. 7).

3.3. Misfit Localization and Defect Structure

The strength of the interatomic interaction across the interface is expected to be largely determining the degree of misfit localization. In contrast to this, the misfit is a purely geometric quantity, which determines the quasiperiod of the misfit structures, as long as the interface is free of residual strains. As the amount of misfit changes from one system to the other, interfaces also show different interface structures. Moreover, different atomic-scale interface structures may be found in the same system, depending on processing conditions or other factors.

Figure 1 shows a (111) interface of a Cu precipitate in NiO, viewed along $<0\bar{1}1>$. Although the misfit is quite large ($|\eta|=0.14$), a definite modulation in the structure of the interface can be recognized. The observed structural period corresponds to the expected spacing of the network of misfit dislocations. The misfit also appears to be distributed over

several (111) planes on the Cu side and one can see that the (111) Cu lattice fringes in the region of misfit do not fully meet the NiO plane. More detailed observations and comparisons to atomic models via image simulations will be necessary to determine the true nature of the misfit localization and the role of point defects. Certainly, the introduction of vacancy-type defects may be able to minimize the interfacial energies for large misfit boundaries that have strong enough bonding for the coherence to be maintained over part of the interface.

A stand-off effect, i. e. when the misfit dislocation terminates at a short distance from the interface, was first observed for the Nb/Al_2O_3 interface [9]. Presumably, the energy of the interface is minimized by maintaining perfect coherence for the first metal layer, while the misfit dislocation is formed at some distance from the interface. Recent observations of stand-off-free Nb/Al_2O_3 interfaces prepared by MBE [14] suggest that the preparation conditions may have an important influence on interfacial structure.

The Ni/Ag system ($|\eta| = 0.15$), which has a similar misfit as the NiO/Cu system, gives somewhat delocalized misfit dislocation cores (see Fig. 5), but does not show the stand-off effect. The HREM images are in this case in reasonably good agreement with image simulations based on embedded atom calculations of this interface [3].

The NiO/Pd system, with $|\eta| = 0.071$, lies in the intermediate misfit range, and shows rather complex HREM images, as seen in Fig. 2 a. The atomic column contrast appears to be strongly affected in the vicinity of the interface. On the Pd side of the interface strain contrast effects can be recognized in Fig. 2 a. In this intermediate misfit range the misfit dislocation network is still small enough to produce strong overlap between misfit dislocations within the thickness of the sample, while the strain fields also reach far enough to affect several atomic planes in the immediate vicinity of the interface.

It is useful to compare the observed images with multislice calculations for a rigid model of this interface. In the model chosen the interface is incoherent and it was assumed that the interface is formed between (111) oxygen and palladium planes with a Pd-O bond

length of 0.201 nm, as found in PdO. Two dimensional periodicity in the interface plane was imposed by a slight adjustment (0.2 %) of the Pd lattice parameter. The EMS suite of programs [15] was used for the image simulations. The boundary supercell (7.66x7.16x4.13 nm) contained 11106 atoms. Multislice calculations were performed with an array of 1024x1024 sampling points up to a total thickness of 12.4 nm. Imaging parameters appropriate for the experimental conditions at the H9000 were used ($C_s = 0.9$ mm, convergence semi angle $\alpha = 0.9$ mR, objective aperture radius $r_{obj} = 5.9$ nm^{-1}).

Fig. 2 b shows comparisons between experimental and simulated images for a thickness of 6.5 nm and 3 focal steps. One notes that the HREM observations of the Pd/NiO interface reflect to a considerable degree the periodic contrast features associated with the incoherent interface. This points immediately to the complexity of extracting information on the distribution of misfit from HREM observations in this misfit range. Although it is clear, particularly from the appearance of periodic strain contrast features, that the interface is not incoherent, the degree of misfit localization cannot be simply extracted from the HREM observations. Since even the image simulations for the incoherent structure were quite large (94 CPU hrs on a 3520 Vax workstation), simulations involving the detailed variation of the atomic displacements in the vicinity of the interface would be considerably more complex. It may therefore not be feasible to try to construct a model of this interface from HREM observations alone. Nevertheless, more detailed information on the interface could be obtained from rigid model simulations. Note for example that the Fresnel-type contrast effect in Fig 2b at a defocus of -14.3 nm is not well matched and could be due to a small rigid-body translation.

The TiO_2/Al_2O_3 system along the $<10\bar{1}>_R$ direction has a misfit ($|\eta| = 0.059$) comparable to the NiO/Pd system, however displays a completely different structure, as illustrated in Fig. 9. Here the coherence of the atomic planes in between the misfit dislocations is so strong that it is difficult to recognize the actual interface plane. The misfit is very strongly localized at and about the misfit dislocation cores. In this projection, the

HREM analysis should not be significantly affected by the presence of a two-dimensional misfit dislocation network because the misfit in the direction of the electron beam is very small (see table 1.). However, due to the very large strains (note strain contrast effects in Fig. 9) that accompany the dislocations, or possibly due to reconstruction in the dislocation cores, atomic column contrast is not maintained in the dislocation cores and therefore their detailed atomic structure could not be determined.

NiO/Ag interfaces which were produced by a thin film technique (see 2.1.2.) have a relatively small misfit, $|\eta| = 0.022$, and are characterized by a cube-on-cube orientation. In this system (111) interfaces are preferred, however owing to the special method of preparation, nonequilibrium interfaces are also found. Such a boundary is shown in Fig. 4, where the arrows indicate the position of the interface. On a large scale, the interface is curved and incorporates isolated misfit dislocations. A stand-off distance of 2-3 interplanar spacings is observed in Fig. 4 . The misfit dislocations appear fairly well localized in this system [3] and the bending of the (111) planes crossing the interface can be clearly recognized in Fig. 4. The TiO_2/Al_2O_3 system along the $<010>_R$ direction has the smallest misfit investigated here ($|\eta| = 0.005$) and shows perfect coherence at practically all planar sections of the interface, an example of which is shown in Fig. 8. The misfit in this case is largely taken up at defects associated with steps in the substrate.

MgO/Au interfaces have a misfit $|\eta| = 0.032$ if the lattices are in the cube-on-cube orientation. Since this is not the case for the smoke particle experiment, a range of boundaries exist with different misfits, depending on their geometry. The boundary in Fig. 7a , for example, matches (200) MgO planes with (111) Au planes, resulting in a quite large misfit ($|\eta| = 0.11$). Misfit localization is also observed at this interface. Atomically well-matched regions can also be observed in Fig. 7b, which shows the transition from one facet to the next at a curved part of a MgO/Au interface.

4. Discussion and Conclusions

The dominance of (111) faces in all fcc systems that have been fully equilibrated indicates that interfaces formed by these dense-packed planes have low energy. This is in agreement with theoretical considerations [16] and some observations in grain boundaries,where dense-packed planes appear to be preferred energetically in ceramics as well as metals [17 - 19]. The rutile/sapphire interfaces investigated here are also formed by dense-packed planes. Whereas in a metal/metal system the close-packing of atoms may be the dominant feature to accomplish a low-energy configuration, (111) planes are charged in the oxides and oxygen anions alternate with (111) metal cation planes. While the electrostatic dipole moment of these interfaces will be largely compensated by induced charges in the metal [20], a net charge on the precipitates also needs to be avoided for energetic reasons. Hence, these interfaces most likely must incorporate defects on the oxygen sublattice, but unfortunately these are not expected to be visible by HREM due to the weak scattering potential of oxygen.

Therefore, the atomic structure of metal/ceramic interfaces must be considerably more complex than equivalent metal boundaries. Nevertheless, on the level of qualitative HREM, we have seen considerable similarities between these systems. An important issue concerns the nature and strength of the cohesive forces and the degree of localization of the interactions across the interface. Coherence is generally understood as the continuation of lattice planes and lines across the interface [21], while no correspondence between atomic positions across the interface exists for an incoherent interface. The tendency to establish coherence reflects the localization of the *atomic* interactions, while the strength of the interactions should determine the degree of *misfit* localization.

Misfit dislocations on (111) heterophase boundaries are expected to form a hexagonal network [22], as observed for example in the epitaxy of Pd on Au [23]. Here edge type dislocations of Burgers vector $b=a/2\langle 1\bar{1}0\rangle$ with line vectors $\langle 11\bar{2}\rangle$ form a

network of dislocations, two of which are inclined by 30° to the <110> HREM viewing direction and one of which is perpendicular to $<0\bar{1}1>$. The unit cell dimensions of this pattern perpendicular and parallel to $<0\bar{1}1>$ (d_n , d_p) in nm would be (3.3, 1.9) and (6.9, 4.1) for NiO/Cu and Pd/NiO respectively. Clearly, such an arrangement of defects in the interface is expected to disturb the atomic column contrast in HREM images. A similar network of relaxations has been calculated, using EAM potentials, for the (111) interface in Ni/Ag [3]. In this instance the interactions are relatively weak and therefore the misfit dislocations are not strongly localized. Although a delocalization of the misfit may be implied from the HREM image of a misfit dislocation in this system, as shown in Fig. 5, simulated HREM images based on the EAM calculations show extremely subtle contrast effects. Quantitative comparisons therefore must be based on matching of through-focal series and may still only be able to discriminate between strongly different model structures. On a qualitative level, the periodic contrast features seen in metal/ceramic interfaces appear typically stronger (see Figs. 1 and 2), which may result from the fact that in metal/metal boundaries the elastic constants are usually not widely different, while in metal/ceramic systems the relaxations are often largely limited to the softer metal side.

While in contrast to metal/metal systems, detailed atomic models of the misfit localization in metal/ceramic systems are not available at this point, HREM has nevertheless been very valuable for observing possible defect configurations. It has been shown first in the Nb/Al_2O_3 system that the tendency to produce coherency directly at the interface can be strong enough to have a stand-off distance for the misfit dislocation [9], which can be understood in terms of minimizing the elastic energy of the system [24]. The observations on Ag/NiO suggest that such a stand-off effect may also be typical for fcc metal/ceramic systems. It is interesting to note that considerable variations in the atomic relaxations are possible even within the same system. Interfaces with and without the stand-off effect have been observed in the Nb/Al_2O_3 system [9,14]. This points to the important role that

processing conditions, point defects and impurities may play in the formation of the interfacial structures between a metal and a ceramic.

Within the systems investigated here no evidence for the formation of a second phase at the interface was found. The possibility of a reconstruction of the misfit dislocation cores, including differing chemical compositions can however not be excluded, particularly in complex structures. In analogy we only mention here the reconstruction of grain boundary dislocation cores in $YBa_2Cu_3O_{7-x}$ [25]. A reconstruction could, for example, be associated with the rather strong contrast effects seen in Fig. 9 for the TiO_2/Al_2O_3 interface. Clearly, for a full understanding of interfacial structure there is a need for atomic-scale chemical analysis of the interfacial region and interface defects.

The observation for Pd/NiO that the precipitates form in the cube-on-cube orientation as well as in the twin related orientation may have significance concerning the range of the interatomic interactions across the interface. From the fact that the precipitates can nucleate on (111) planes in the cube-on-cube as well as on the twin related orientation, it appears that a reversal of the stacking sequence in the oxide is of only minor influence on the interfacial energy. Such a behavior could be explained if the interatomic interactions across the interface are extremely short range, i. e. if second nearest neighbor interactions can be neglected [11]. Precipitates with fully twin related orientation, albeit with a reduced probability, have also been observed by Lu and Cosandey in the Pd/MgO system [26].

5. Summary

HREM studies on heterophase interfaces in metal/metal, metal/ceramic, and ceramic/ceramic boundaries have shown a tendency for establishing coherence across the boundary in all of the systems studied here.

In all fcc systems (111) interfaces appear to be preferred energetically.

Interfaces prepared by a variety of techniques, including internal reduction, internal oxidation, and epitaxial growth by MOCVD and special thin-film techniques show considerable similarities in the way in which the misfit is being accommodated.

The degree of coherency differs from system to system and appears to depend both on the amount of misfit and the bond strength.

The local defect structure at the boundary and the type of misfit localization also seems to depend on processing conditions and substrate defects.

Quite short-range interatomic interactions at the metal/oxide interface may be indicated by the nucleation of NiO on (111) planes in Pd also in the reverse stacking order.

There are considerable difficulties in applying HREM to a detailed determination of the atomic structure of (111) metal/ceramic interfaces in fcc systems, since misfit dislocations are inclined to the <011> zone axis and image simulations based on suitable theoretical models are, in contrast to metal/metal systems, not available at present.

Acknowledgements —— The authors would like to thank J. P. Shaffer for help with multislice calculations and acknowledge fruitful discussions with D. Wolf. The use of the H 9000 at Northwestern University and the technical assistance of J. F. Reddy and C. L. Wiley at Argonne is gratefully acknowledged. This work was supported by the U.S. Department of Energy, Basic Energy Sciences under contract No. W -31-109-ENG-38.

References

1. See in **Metal-Ceramic Interfaces**, M. Rühle, A. G. Evans, M. F. Ashby and J. P. Hirth, eds., Acta-Scripta Metallurgica Proceedings **4**, Pergamon Press (1990) .
2. See in **Intergranular and Interface Boundaries in Materials**, Colloque de Physique **51**, Les Éditions de Physique (1990) .
3. Y. Gao and K. L. Merkle, J. Mater. Res. **5**, 1995 (1990).
4. Y. Gao and K. L. Merkle, Mater. Res. Soc. Proc. **183**, 39 (1990).
5. H. L. M. Chang, H. You, J. C. Parker and D. J. Lam, Applied Surface Science **48/49**, 12 (1991).
6. S. Mahajan and L. Himmel, Acta Metall. **20**, 1313 (1962).
7. D. J. Pedder, Metal. Trans. **9 A**, 659 (1978).
8. G. Necker and W. Mader, Phil. Mag. Lett. **58**, 205 (1988).
9. W. Mader and G. Necker, in **Metal-Ceramic Interfaces**, M. Rühle, A. G. Evans, M. F. Ashby and J. P. Hirth, eds., Pergamon Press (1990) p. 223 .
10. F. Ernst, P. Pirouz and A. H. Heuer, Mater. Res. Symp. Proc. **138**, (1989).
11. K. L. Merkle, in **Metal-Ceramic Interfaces**, M. Rühle, A. G. Evans, M. F. Ashby and J. P. Hirth, eds., Pergamon Press (1990) p. 242 .
12. Y. Gao, K. L. Merkle, H. L. M. Chang, T. J. Zhang and D. J. Lam, Mater. Res. Soc. Symp. Proc. **209**, 685 (1991).
13. Y. Gao, K. L. Merkle, H. L. M. Chang, T. J. Zhang and D. J. Lam. J. Mater. Res. in press (1991).
14. J. Mayer, W. Mader, D. Knauss, F. Ernst and M. Rühle, Mater. Res. Symp. Proc. **183**, 55 (1990).
15. P. Stadelmann, Ultramicroscopy **21**, 131 (1987)
16. D. Wolf, J. de Physique **46**, 197 (1985).

17. K. L. Merkle and D. J. Smith, Ultramicroscopy **22**, 57 (1987).

18. K. L. Merkle and Y. Gao, in **Microbeam Analysis-1991**, D. G. Howitt, ed., San Francisco Press, San Francisco (1991) p. 207 ; K. L. Merkle, Ultramicroscopy **37**, 130 (1991).

19. K. L. Merkle and D. Wolf, MRS Bulletin **15**, 42 (1990)

20. M. W. Finnis, A. M. Stoneham and P. W. Tasker, in **Metal-Ceramic Interfaces**, M. Rühle, A. G. Evans, M. F. Ashby and J. P. Hirth, eds., Pergamon Press (1990) p. 35 .

21. J. W. Christian. **Dislocations and Phase Transformations**, (The Institute of Metals, London, 1985) ; G. B. Olson and M. Cohen. Acta Metall. **27**, 1907 (1979).

22. W. Bollmann, **Crystal defects and crystalline interfaces,** (Springer, Berlin, 1970) .

23. K. Jagi, K. Takajanagi, K. Kobayashi and G. Honjo, J. Cryst. Growth **9**, 84 (1971).

24. S. V. Kamat, J. P. Hirth and B. Carnahan, Mater. Res. Soc. Symp. **103**, 55 (1988).

25. Y. Gao, K. L. Merkle, G. Bai, H. L. M. Chang and D. J. Lam, Physica C **174**, 1 (1991).

26. P. Lu and F. Cosandey, Acta Metallurgica et Materalia, this conference.

Table 1. The absolute value of the misfit η (with $\eta=2(b_1-b_2)/(b_1+b_2)$, where b_1 and b_2 are the interatomic distances along the boundary for the matrix and substrate or the precipitate and overlayer respectively) covers a wide range for the interfaces investigated. For fcc systems, cube-on-cube orientation is assumed.

Interface	Misfit $\lvert\eta\rvert$
NiO/Cu	0.144
NiO/Pd	0.071
NiO/Ag	0.022
MgO/Au	0.032
Ni/Ag	0.15
TiO_2/Al_2O_3	$<10\bar{1}>_R$ 0.005
$(101)_R \parallel (11\bar{2}0)$	$<010>_R$ 0.059

Figure Captions

Fig. 1. HREM image of NiO/Cu (111) interface produced by internal reduction.

Fig. 2. HREM images of (111) NiO/Pd interface in the cube-on-cube orientation, produced by internal oxidation, viewed in $<1\bar{1}0>$ direction. a) Complex interface image. Note periodic strain contrast features on Pd side. b) Through-focal series with ΔF indicated on bottom. Top: Experimental images. Bottom : Simulated images for rigid model. (H9000, 300 kV, $C_s = 0.9$ mm, $\alpha = 0.9$ mR, $r_{obj} = 5.9$ nm^{-1}).

Fig. 3. HREM image of part of a NiO precipitate (top) produced by internal oxidation in Pd.

Fig. 4. HREM image of a non-equilibrium NiO/Ag interface prepared by a thin film technique. Interface position indicated by arrows. Note misfit dislocation at stand-off distance.

Fig. 5. HREM image of Ni/Ag interface prepared by a thin film technique. Note matching of (111) planes across boundary outside region of misfit (arrow).

Fig. 6. Ni/Ag (110) interface (arrows) decomposes into (111) microfacets to lower the total interfacial energy [3].

Fig. 7 HREM images of MgO/Au interfaces prepared by thin a film technique, using MgO smoke particles and epitaxially grown Au on NaCl.

Fig. 8. MOCVD grown rutile film (TiO_2) on $(11\bar{2}0)$ sapphire viewed along $<010>_R$. This coherent interfacial region shows perfect lattice match. The interface is indicated by arrows and can be recognized by the change in direction of the lattice planes crossing the interface.

Fig. 9. MOCVD grown TiO_2 on $(11\bar{2}0)$ sapphire viewed along the $<10\bar{1}>_R$ direction in the rutile film. Note strong misfit localization.

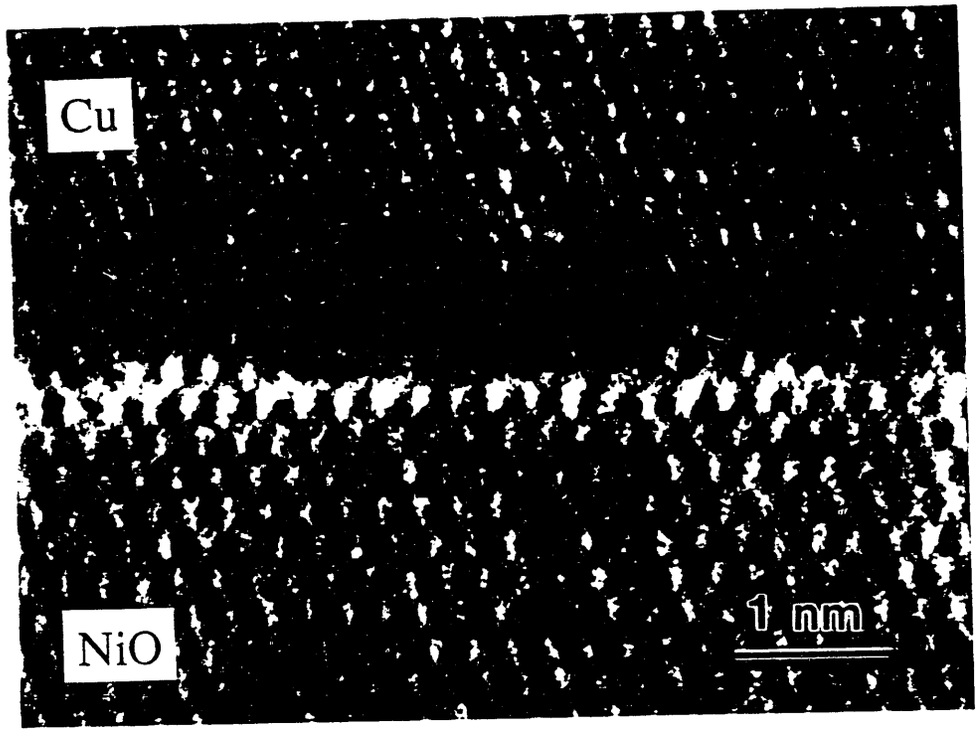

Fig. 1

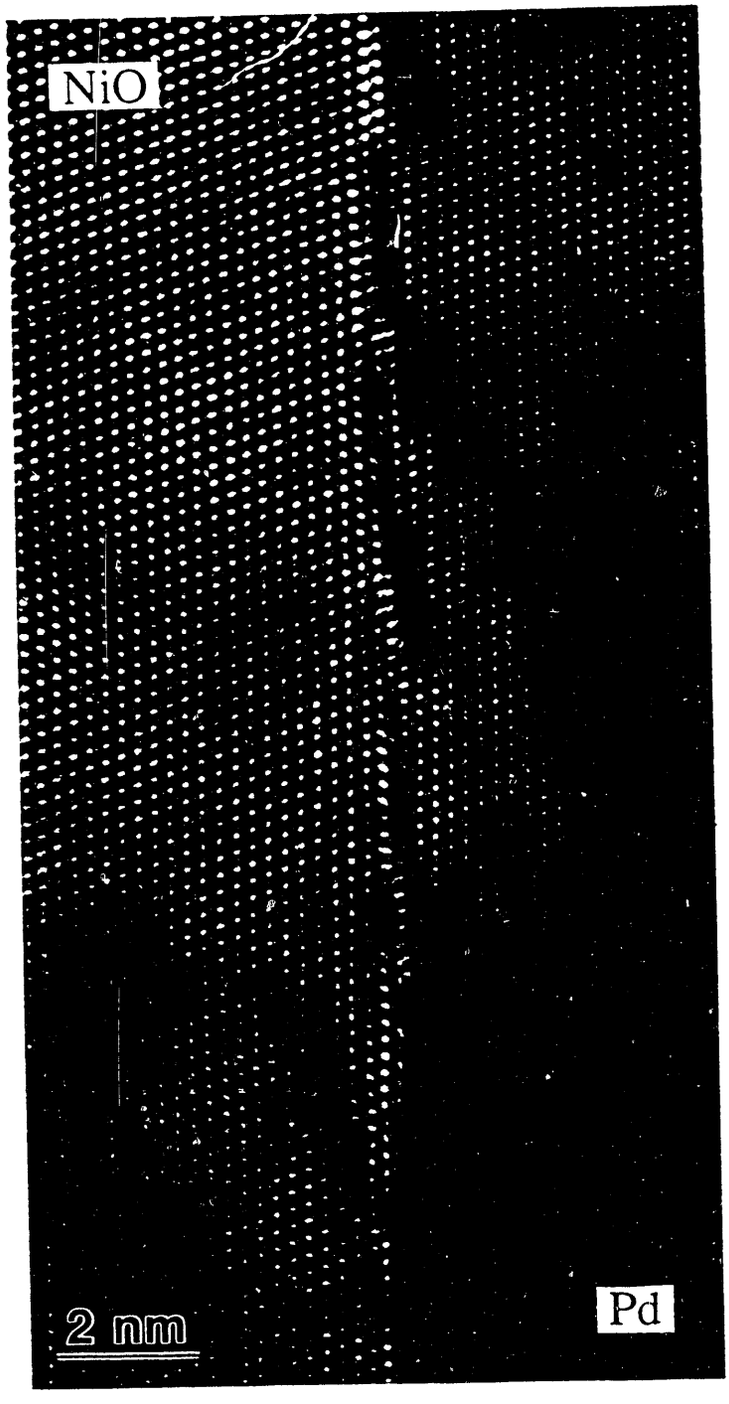

Fig. 2a

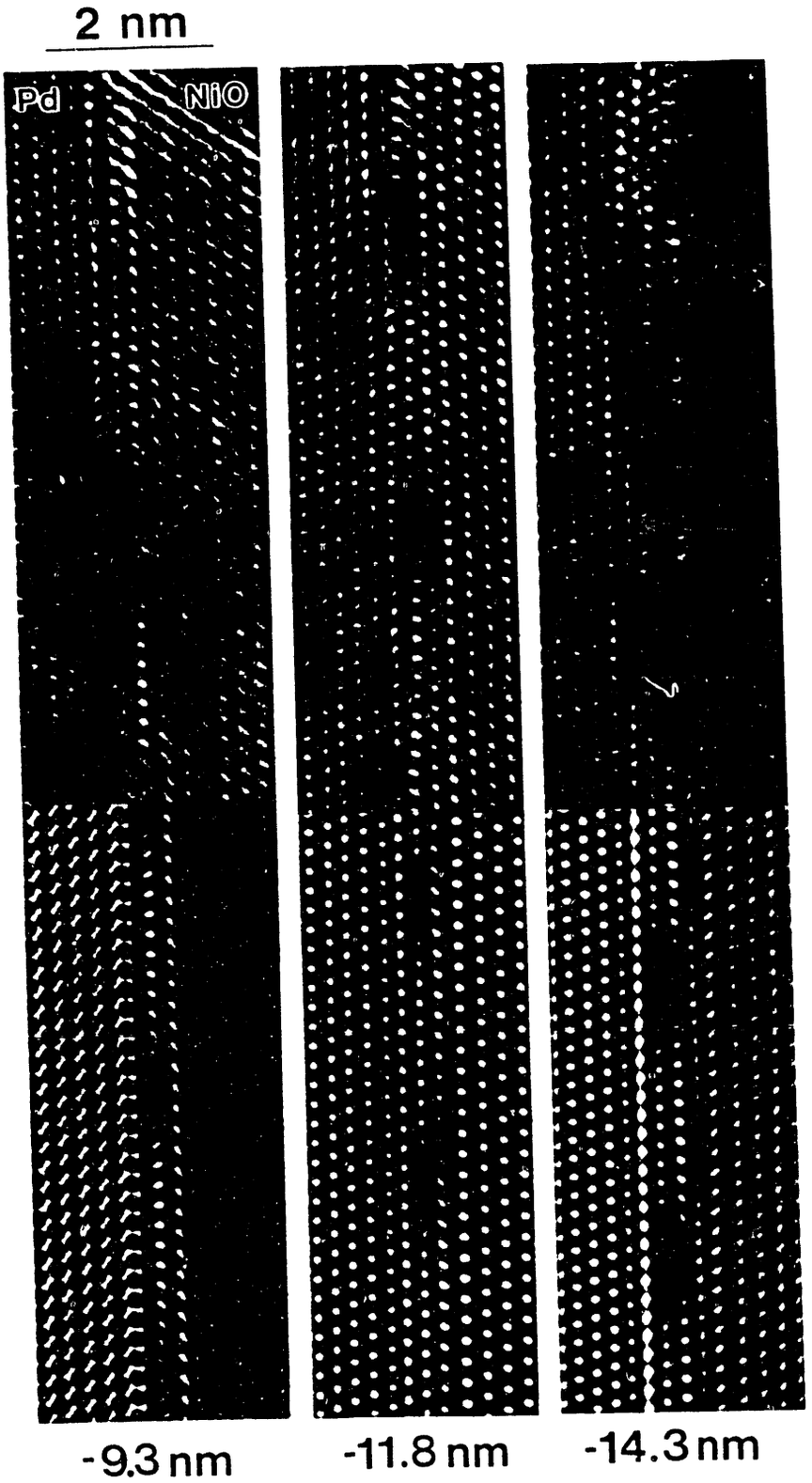

Fig- 2b

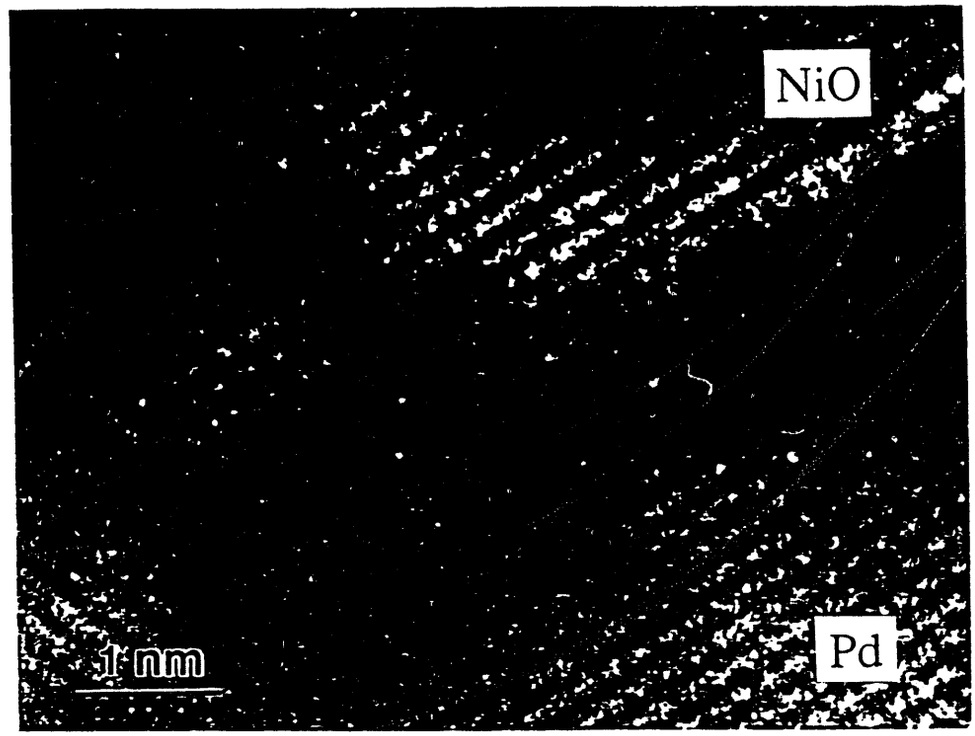

Fig. 3

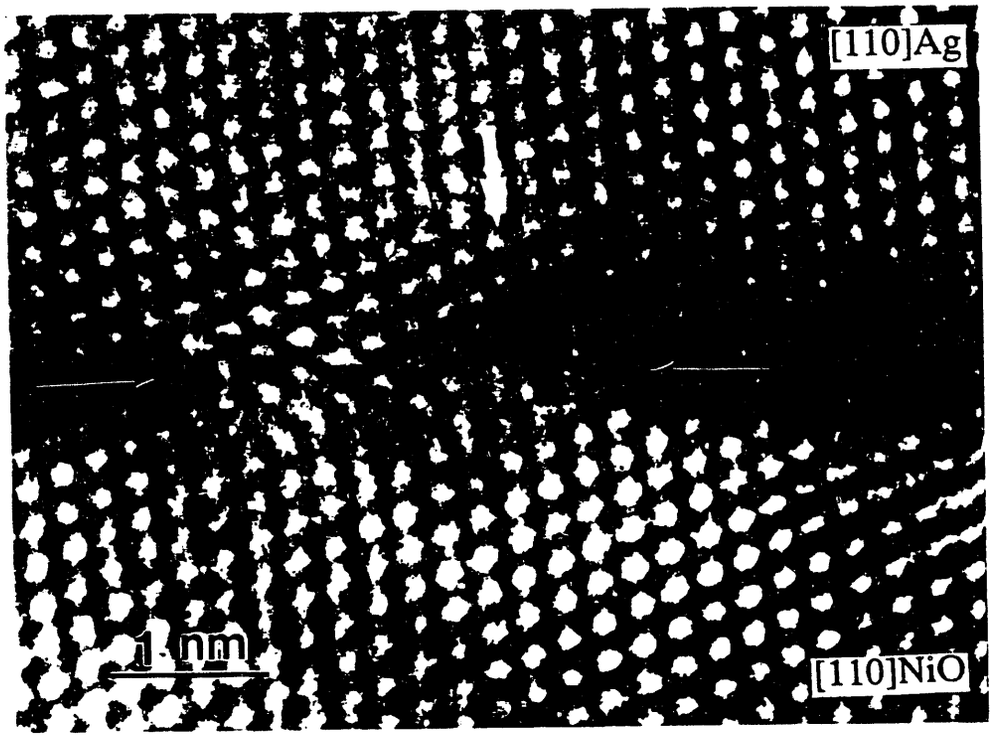

Fig. 4

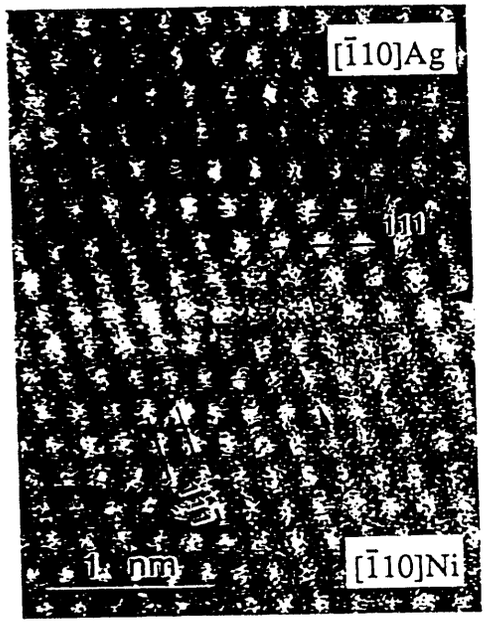

Fig. 5

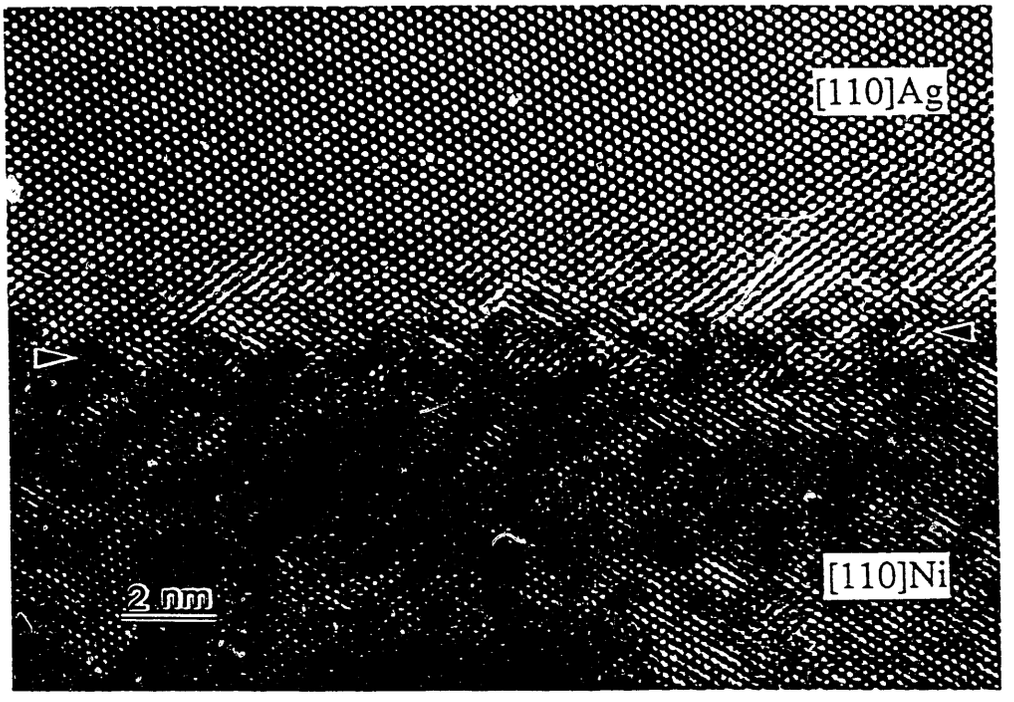

Fig-6

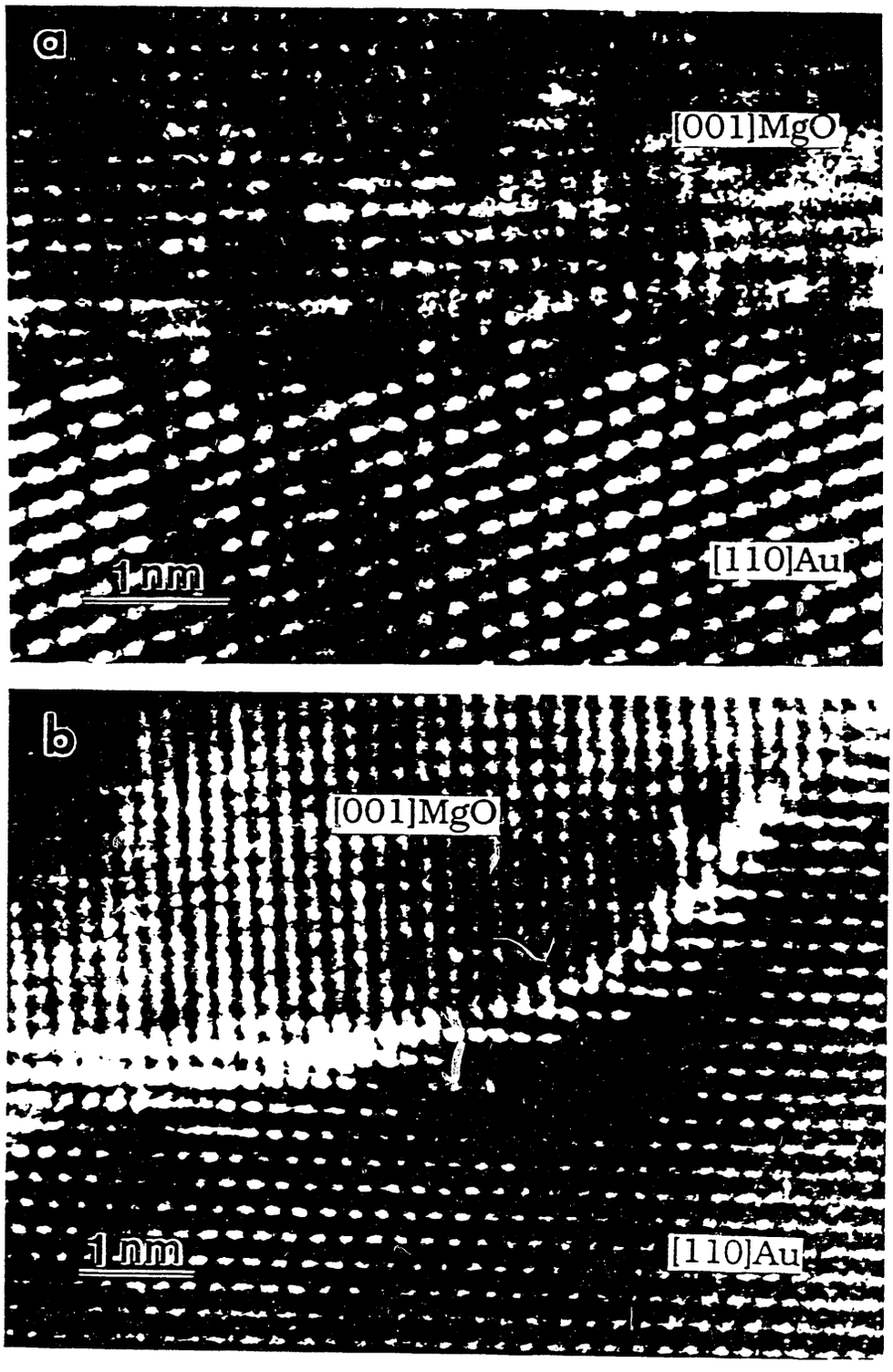

Fig. 7

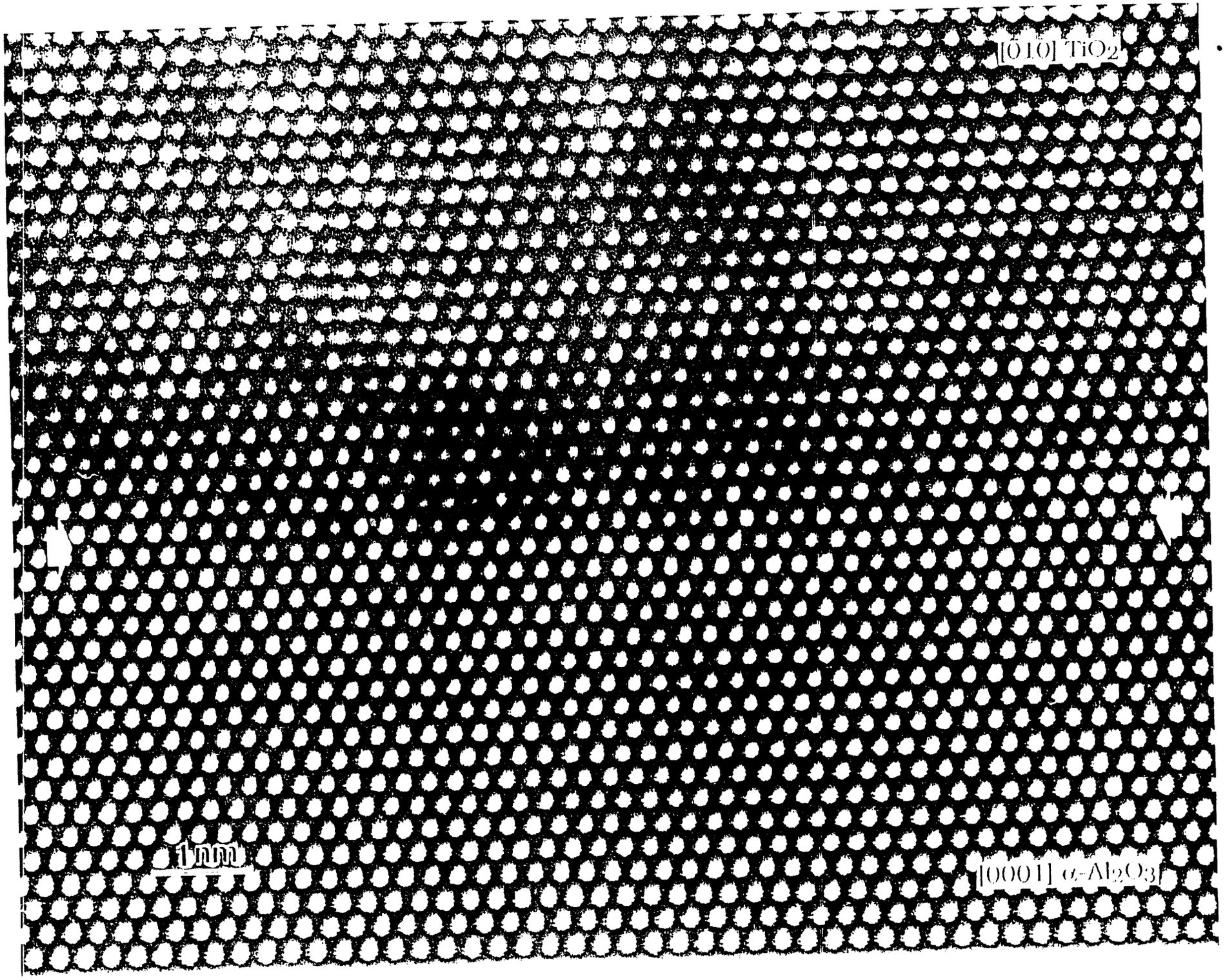
[010] TiO_2
1 nm
[0001] α-Al_2O_3

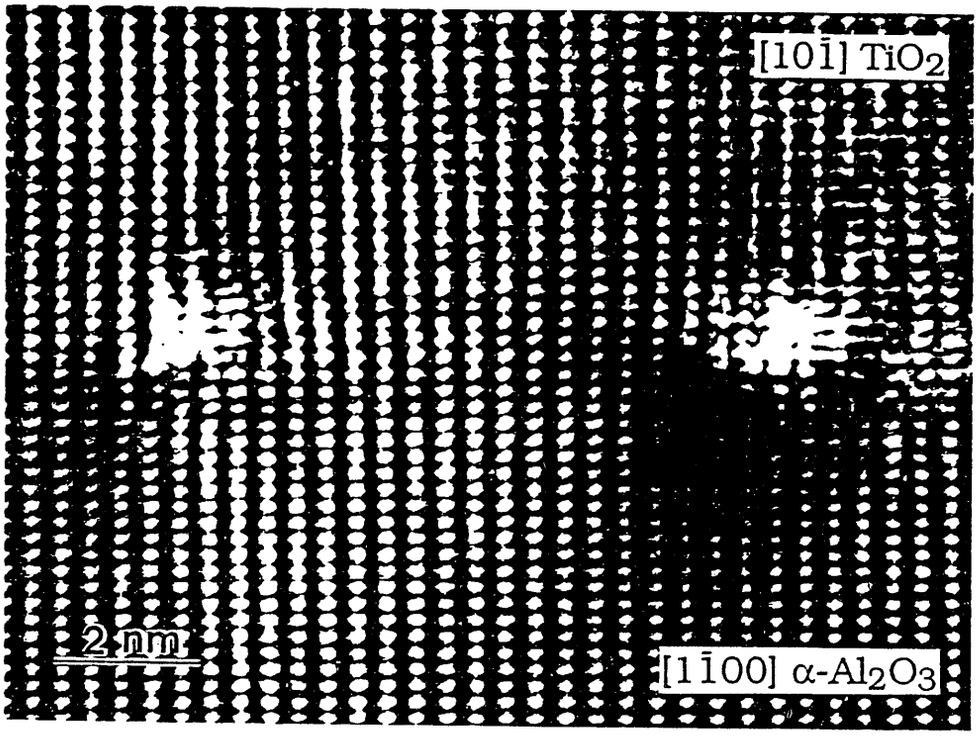

Fig. 9

END

DATE FILMED

7/8/92